occupancy in schizophrenic patients. *Am J Psychiatry.* 1999;156:869–875.

31. Saruwatari J, Yasui-Furukori N, Inoue Y, et al. Effect of dose timing in relation to food intake on systemic exposure to blonanserin. *Eur J Clin Pharmacol.* 2010;66:899–902.
32. Arakawa R, Ito H, Takano A, et al. Dose-finding study of paliperidone ER based on striatal and extrastriatal dopamine D_2 receptor occupancy in patients with schizophrenia. *Psychopharmacology (Berl).* 2008;197:229–235.
33. Halldin C, Farde L, Högberg T, et al. Carbon-11-FLB 457: a radioligand for extrastriatal D_2 dopamine receptors. *J Nucl Med.* 1995;36:1275–1281.
34. Arnt J, Skarsfeldt T. Do novel antipsychotics have similar pharmacological characteristics? A review of the evidence. *Neuropsychopharmacology.* 1998;18:63–101.
35. Agid O, Mamo D, Ginovart N, et al. Striatal vs extrastriatal dopamine D_2 receptors in antipsychotic response—a double-blind PET study in schizophrenia. *Neuropsychopharmacology.* 2007;32:1209–1215.
36. Kessler RM, Ansari MS, Riccardi P, et al. Occupancy of striatal and extrastriatal dopamine D_2/D_3 receptors by olanzapine and haloperidol. *Neuropsychopharmacology.* 2005;30:2283–2289.
37. Kessler RM, Ansari MS, Riccardi P, et al. Occupancy of striatal and extrastriatal dopamine D_2 receptors by clozapine and quetiapine. *Neuropsychopharmacology.* 2006;31:1991–2001.
38. Farde L, Hall H, Pauli S, et al. Variability in D2-dopamine receptor density and affinity: a PET study with [11C]raclopride in man. *Synapse.* 1995;20:200–208.
39. Kessler RM, Meltzer HY. Regional selectivity in clozapine treatment? *Am J Psychiatry.* 2002;159:1064–1065.
40. Ito H, Arakawa R, Takahashi H, et al. No regional difference in dopamine D_2 receptor occupancy by the second-generation antipsychotic drug risperidone in humans: a positron emission tomography study. *Int J Neuropsychopharmacol.* 2009;12:667–675.
41. Narendran R, Mason NS, May MA, et al. Positron emission tomography imaging of dopamine D_2/D_3 receptors in the human cortex with [^{11}C]FLB 457: reproducibility studies. *Synapse.* 2011;65:35–40.

Psychiatry and Clinical Neurosciences 2013; 67: 3–11 doi:10.1111/pcn.12003

Regular Article

Effects of menopause on brain structural changes in schizophrenia

Hajime Fukuta, MD,[1] Itsuo Ito, MD,[1] Amane Tateno, MD, PhD,[1] Tsuyoshi Nogami, MD,[1] Yasutomo Taiji, DipMedLab,[2] Ryosuke Arakawa, MD, PhD,[3] Tetsuya Suhara, MD, PhD,[3] Kunihiko Asai, MD[2] and Yoshiro Okubo, MD, PhD[1]*

[1]*Department of Neuropsychiatry, Nippon Medical School, Tokyo,* [2]*Asai Hospital and* [3]*Molecular Neuroimaging Group, Molecular Imaging Center, National Institute of Radiological Sciences, Chiba, Japan*

Aim: The aim of this study was to investigate the influences of menopause on brain morphological changes in schizophrenia using magnetic resonance imaging (MRI).

Methods: Forty female schizophrenia patients, 20 premenopausal and 20 postmenopausal, and 50 female controls underwent cerebral MRI. Optimized voxel-based morphometry was performed with Statistical Parametric Mapping version 5.

Results: Compared with controls, regional gray matter reductions in schizophrenia patients were observed in the insula, superior temporal gyrus, anterior cingulate, parahippocampal gyrus, and thalamus. Direct comparison between the patient groups showed that the gray matter of postmenopausal patients was significantly smaller when compared with premenopausal patients in the left middle frontal gyrus, and no region had significantly lower gray matter volume in premenopausal patients relative to postmenopausal patients. Significant negative correlation between gray matter volume and the interval after menopause was found in the right superior frontal gyrus in the postmenopause patient group.

Conclusion: Differential morphological alterations between postmenopausal and premenopausal schizophrenia patients were observed, suggesting that the female hormone plays a protective role against schizophrenia.

Key words: brain morphology, estrogen, female, menopause, schizophrenia

MANY STUDIES HAVE indicated the vulnerability to the pathological process of male schizophrenia patients relative to female patients. Female schizophrenia patients have lower antipsychotic dosage,[1] and a less malignant course of illness[2] than male patients. In addition, several studies have reported that schizophrenia has a later onset in female patients, with the first peak of onset in female patients occurring at age 25–29 years, in contrast to the peak of onset in male patients at age 20–24 years.[3] In addition, a second smaller peak of onset occurs in women after age 44 years, around perimenopause and menopause.[4,5] Based on these findings, it had been hypothesized that estrogen exerts a protective effect against the pathological process in schizophrenia.[5]

Studies regarding gender differences of brain morphology in schizophrenia had demonstrated more vulnerability in male patients than female patients. Magnetic resonance imaging (MRI) and postmortem studies have reported a tendency of greater abnormalities in male patients,[6] and male patients had larger lateral ventricle[6] and smaller medial temporal volume, that is, hippocampus and amygdala,[7] superior temporal gyrus,[7–9] and frontal[9] and temporal[10]

**Correspondence:* Yoshiro Okubo, MD, PhD, Department of Neuropsychiatry, Nippon Medical School, 1-1-5 Sendagi, Bunkyo-ku, Tokyo 113-8603, Japan. Email: okubo-y@nms.ac.jp*
Received 2 October 2011; revised 13 June 2012; accepted 15 June 2012.

lobe volumes than normal controls. Although these findings related to gender differences cannot be explained only by the degree of estrogen level, it could be hypothesized that the effect of estrogen partly reduces brain morphological changes in schizophrenia.

To our knowledge the relationship between estrogen and brain morphology in schizophrenia has not been reported in previous studies, although in postmenopausal female subjects without schizophrenia, several studies have reported the effect of estrogen therapy on brain atrophy.[11–13]

If female patients are under hormonal protection that can reduce the particular brain morphological changes of this disease, it could be suggested that premenopausal patients are under similar protection relative to postmenopausal patients. This would explain why only female patients have a second peak of onset in the paramenopausal phase.

In this study, we examined the influences of menopause on brain morphological changes of schizophrenia patients by classifying them into two subgroups, postmenopausal and premenopausal, using MRI. Although there is no previous study that investigated the effect of menopause on brain morphology of schizophrenia, studying gray matter (GM) volume by voxel-based morphometry (VBM)[14] has helped detect the localized effects of clinical characteristics, such as symptoms,[15] duration of illness,[16] and antipsychotic treatment,[17] and we considered VBM suitable for this investigation. We also examined whether the volumetric changes of postmenopausal patients were related to years elapsed after menopause.

METHODS

Subjects

Twenty female schizophrenia patients whose interval between last menstruation and the present MRI was at least 12 months were recruited and classified as the postmenopausal patient group. For the premenopausal patient group, 20 female schizophrenia patients matched to the postmenopausal patient group by age, and who had an interval between their last menstruation and the present MRI <12 months, were recruited.

The menstrual state of all patients was checked by interview. Twelve consecutive months of amenorrhea is the epidemiological definition of menopause according to Treloar.[18]

All patients fulfilling the diagnosis of schizophrenia as defined by DSM-IV criteria were recruited from the inpatient and outpatient facilities of Asai Hospital, Chiba, Japan. Diagnoses were made by the attending psychiatrists on the basis of a review of their charts and a conventional, semi-structured interview. In the 20 premenopausal patients, schizophrenia diagnosis was as follows: paranoid subtype, $n = 12$; disorganized subtype, $n = 1$; catatonic subtype, $n = 1$; undifferentiated subtype, $n = 1$; and residual subtype, $n = 5$. In the 20 postmenopausal patients the diagnosis was as follows: paranoid subtype, $n = 13$; disorganized subtype, $n = 0$; catatonic subtype, $n = 2$; undifferentiated subtype, $n = 2$; and residual subtype, $n = 3$, based on DSM-IV criteria.

The comparison group consisted of 50 healthy female volunteers matched with the patient groups by age, exclusion being based on a history of DSM-IV axis I or axis II disorder. Patients and comparison subjects were excluded if they had a history of head injury, neurological illness, or a diagnosis of substance abuse or dependence. Demographic and clinical characteristics are listed in Table 1.

All subjects were within the limited age range of 30–59 years. The mean age of premenopausal patients was 44.4 ± 8.0 years, postmenopausal patients, 46.8 ± 8.2 years; and normal controls, 45.0 ± 8.7 years. There were no significant differences in age between the groups according to diagnosis and menopause (analysis of variance, $P = 0.63$).

All patients were taking neuroleptic medication. Neuroleptic dosage in the premenopausal group was 959.5 ± 618.5 mg (chlorpromazine equivalent: atypical, $n = 7$; typical, $n = 5$; combined typical and atypical, $n = 8$). The dosage in the postmenopausal group was 746.8 ± 463.5 mg (chlorpromazine equivalent: atypical, $n = 10$; typical, $n = 4$; combined typical and atypical, $n = 6$). There were no significant differences in dosage or ratio of atypical, typical and combined therapy. Further, none of the patients was taking any hormonal therapy or other medication that could influence the level of sex hormones.

Patient symptoms were rated by Global Assessment of Functioning (GAF) and the Brief Psychiatric Rating Scale (BPRS).[19] BPRS total scores, as well as positive symptom (conceptual organization, unusual thought content, hallucinatory behavior) and negative symptom (emotional withdrawal, motor

Table 1. Subject characteristics

	Schizophrenia patients		Normal controls
	Premenopause	Postmenopause	
Variable (mean ± SD)	$n = 20$	$n = 20$	$n = 50$
Age (years)	44.4 ± 8.0	46.8 ± 8.2	45.0 ± 8.7
Period after menopause (years).	NA	5.0 ± 5.1	Unknown
Age at onset (years)	22.7 ± 10.6	24.9 ± 8.4	NA
Duration of illness (years)	21.0 ± 11.6	25.0 ± 13.0	NA
No. episodes	5 ± 3.9	7 ± 6.2	NA
GAF score	46 ± 11.0	42 ± 10.4	NA
Total BPRS score	49 ± 15.7	47 ± 18.2	NA
BPRS (P)	11.7 ± 3.9	10.7 ± 3.9	NA
BPRS (N)	9.8 ± 2.9	10.2 ± 4.0	NA
Education (years)	11.2 ± 1.9	11.6 ± 2.1	Unknown
Antipsychotics (*n*)			
Atypical	7	10	NA
Typical	5	4	NA
Combined typical and atypical	8	6	NA
Dosage (mg/day, chlorpromazine equivalent)	959.5 ± 618.5	746.8 ± 463.5	NA
Cumulative dosage (kg, chlorpromazine equivalent)	7.4 ± 7.3	6.3 ± 4.5	NA

BPRS, Brief Psychiatric Rating Scale; GAF, Global Assessment for Functioning; (N), negative symptoms; (P), positive symptoms.

retardation, blunted affect) subscales,[20,21] were used in the present analysis.

There were no significant differences between the patient subgroups in age at onset (two-tailed *t*-test, $P = 0.50$), duration of illness ($P = 0.41$), drug dosage ($P = 0.24$), GAF score ($P = 0.45$), total BPRS score ($P = 0.71$), BPRS positive symptom subscale ($P = 0.48$), negative symptom subscale ($P = 0.75$), or duration of education ($P = 0.46$). The average number of episodes, which represented the times they had been hospitalized because of worsening of their mental conditions, was five for the premenopausal patients and seven for the postmenopausal patients. This difference in number was not statistically significant ($P = 0.28$). Any characteristics except menopause were not significantly different between the patient subgroups.

This study was approved by the ethics committees of Nippon Medical School and Asai Hospital. After complete description of the study, all subjects gave written informed consent.

MRI acquisition

T1-weighted MRI was carried out on a 1.5-T GE Signa scanner (GE Medical Systems, Milwaukee, WI, USA). T1-weighted images were acquired in a coronal plane using an SPGR 3-D imaging sequence with the following parameters: TE = 9 ms, TR = 22 ms, flip angle = 30°, slice thickness = 1.5 mm, field of view = 25 cm, matrix = 256 × 192, voxel dimensions = 0.98 × 0.98 × 1.5 mm.

Image analysis

All images were organized for preprocessing and analyzed using SPM5 (Wellcome Department of Imaging Neuroscience, London, UK. http://www.fil.ion.ucl.ac.uk/spm/software/spm5/) running in MATLAB 2008a (MathWorks, Natick, MA, USA). We used the optimized protocol as detailed by Good *et al.*[22]

We used the customized template of Asai Hospital. It was created from the MRI of 120 healthy subjects (60 male, 60 female) recruited from the local community. All the subjects were within the limited age range of 30–59 years, and were physically healthy at the time of scanning, and none had a history of current or past psychiatric illness, serious head injury, serious medical or neurological illness, or substance abuse.

Each structural MRI from all present schizophrenia and healthy control subjects was segmented into GM,

white matter (WM), and cerebral spinal fluid (CSF) compartments using the SPM priors. An automated brain extraction procedure that incorporated a segmentation step was used to remove non-brain tissue.[22] The extracted GM images were normalized to the created GM template. The normalization parameters obtained from this step were then applied to the original structural images in native space to reduce any contribution from non-brain voxels and afford optimal spatial normalization of GM. These normalized images were segmented into GM, WM, and CSF partitions.

Finally, all normalized, segmented GM images were smoothed with a 12-mm full width at half maximum (FWHM) isotropic Gaussian kernel.

Data analysis

The processed images were analyzed using SPM5. Volumes were compared according to two linear contrasts (more or less GM volume between subject groups).[23]

The resulting set of voxel values for each contrast constituted a statistical parametric map of the t-statistic (SPM-t). Comparisons were made between subject groups, organized by menopause and diagnosis. At first, the GM volume difference between female schizophrenia patients and female controls was investigated using SPM-t maps thresholded at $P < 0.05$ corrected by the family-wise error rate (FWE). Comparison was performed using an analysis of covariance (ANCOVA) model,[24] with age as covariate. We could not check the menopausal state of each of the healthy female subjects. Therefore, this first analysis was to demonstrate the overall tendency of brain morphology in female patients relative to healthy female subjects, without relation to menopause.

Then, the GM volume difference between postmenopausal patients and premenopausal patients was investigated using multivariate analysis of variance with age, antipsychotic medication, duration of illness, and BPRS negative symptoms as covariates (MANCOVA), at $P < 0.001$ uncorrected. The numerical value of the antipsychotic medication was the cumulative exposure calculated by the accumulation of the representative daily dosage of each year of their treatment histories. The representative dosage used was from the longest period of each year. The dosage was multiplied by the treated days of each year, and then accumulated through their treatment histories. The sum of the calculation for premenopausal patients was 7.4 ± 7.3 kg (chlorpromazine equivalent, mean ± SD), and the sum for postmenopausal patients was 6.3 ± 4.5 kg. There was no significant difference between the patient groups ($P = 0.57$).

Further, the relation of brain morphology of postmenopausal patients to years elapsed after menopause was examined using correlation analysis with age as covariate, at $P < 0.001$ uncorrected. Then we performed a region of interest analysis to investigate volume differences of the region significantly correlated with the interval after menopause in each postmenopausal patient, using the Marsbar toolbox.[25]

In the first analysis, we performed a comparison between 40 schizophrenia patients and 50 controls thresholded at $P < 0.05$ corrected. We used a different threshold at $P < 0.001$ uncorrected for the next two analyses, because these were done using a smaller sample size, that is, 20 postmenopausal patients and 20 premenopausal patients for the second analysis and 20 postmenopausal patients for the third analysis.

For visualization of group differences, the coordinates of significant voxels were converted from Montreal Neurological Institute space to Talairach and Tournoux coordinates[26] using a MATLAB conversion program written by Matthew Brett (MRC Cognition and Brain Sciences Unit, UK). Coordinates were then entered into Talairach Daemon[27] to localize results.

RESULTS

Brain regions with significant GM volume change in all analyses are shown in Tables 2–4 and Figs 1,2.

Female schizophrenia patients vs female controls

The regional GM of female schizophrenia patients was significantly smaller when compared with female control subjects ($P < 0.05$ corrected). Significant volume reductions were observed in the bilateral insula, left superior temporal gyrus, bilateral anterior cingulate, left parahippocampal gyrus, and left thalamus (Table 2; Fig. 1a).

No region had significantly lower GM volume in female controls relative to female schizophrenia patients.

Table 2. SPM5 regional GM reduction in patients relative to controls

		Schizophrenia patients < Controls				
			Coordinate			Cluster volume
Anatomical region	[Area]†	T	x	y	z	(mm^3)
Superior temporal gyrus	[41]Lt.	5.04	−46	−24	8	390
Insula	[13]Rt.	5.15	36	16	4	420
	[13]Lt.	6.02	−36	22	0	1880
Parahippocampal gyrus	[34]Lt.	4.98	−18	4	−18	130
Anterior cingulate	[25]Rt.	6.27	2	2	−6	2380
	[25]Lt.	6.39	−4	2	−4	2380
Thalamus	Lt.	5.2	−2	−8	0	2380

†Brodmann area. GM, gray matter; Lt., left hemispheric; Rt., right hemispheric.

Premenopausal patients vs postmenopausal patients

The regional GM of postmenopausal patients was significantly smaller when compared with premenopausal patients at the left middle frontal gyrus (Table 3; Fig. 1b; $P < 0.001$ uncorrected). In contrast, no region had significantly lower GM volume in premenopausal patients compared to postmenopausal patients.

Correlation between brain morphology of postmenopausal patients and interval after menopause

Correlation between brain morphology of postmenopausal patients and the interval after menopause is shown in Table 4 and Figs 1(c),2. The regional brain volume of the right superior frontal gyrus was significantly correlated with the interval after menopause: the longer the interval, the greater

Table 3. SPM5 regional GM reduction vs menopause in schizophrenia

		Postmenopausal patients < Premenopausal patients				
			Coordinate			Cluster volume
Anatomical region	[Area]†	T	x	y	z	(mm^3)
Middle frontal gyrus	[10]Lt.	4.24	−36	40	10	120

†Brodmann area. GM, gray matter; Lt., left hemispheric; Rt., right hemispheric.

Table 4. SPM5 negative correlation between GM volume and period of time after menopause

		Coordinate				Cluster volume
Anatomical region	[Area]†	T	x	y	z	(mm^3)
Superior frontal gyrus	[8]Rt.	4.83	20	38	38	340

†Brodmann area. GM, gray matter; Rt., right hemispheric.

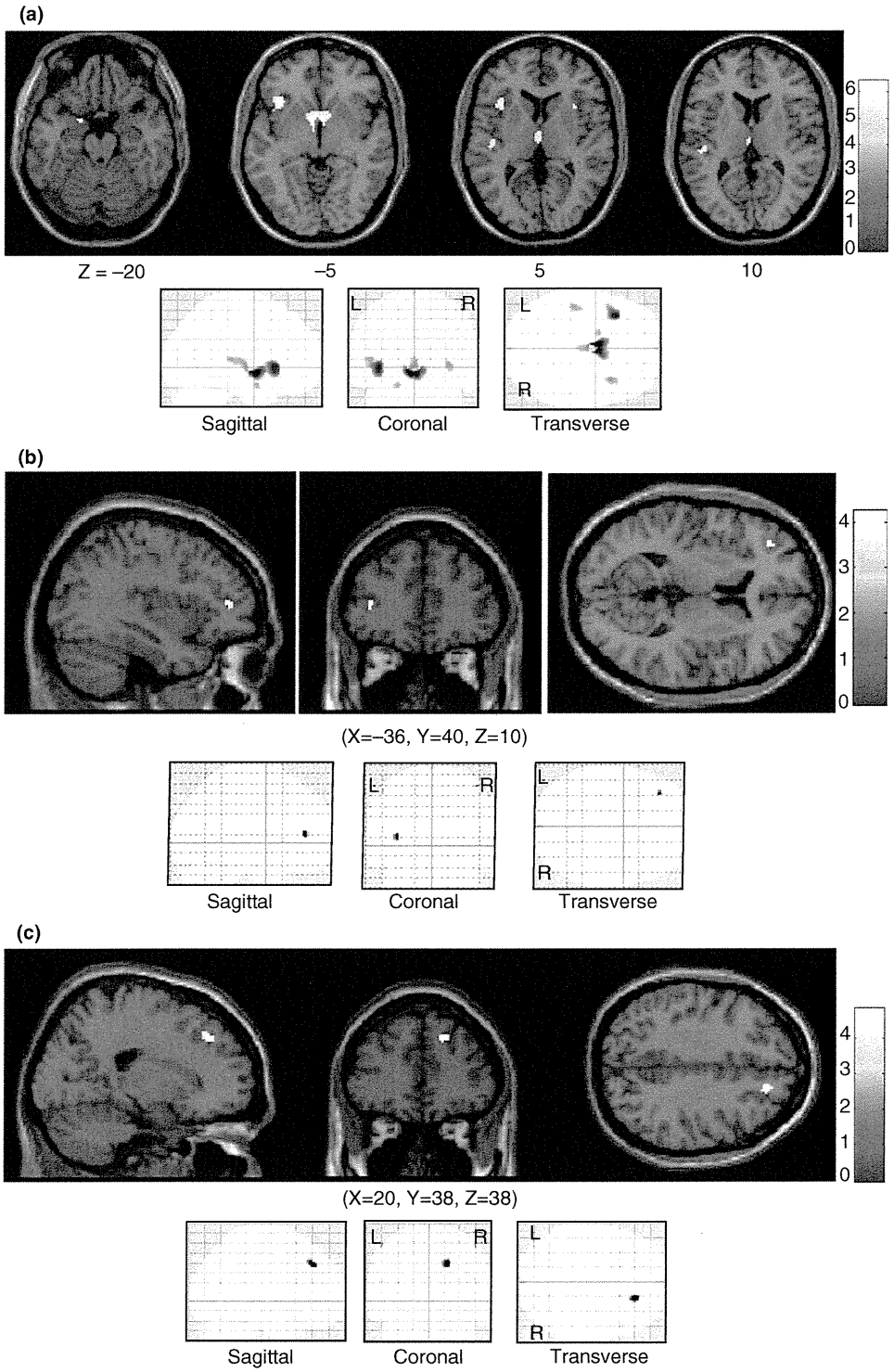

Figure 1. Voxel-based morphometry (VBM) analysis of T contrasts showing gray matter reductions in (a) female schizophrenia patients ($n = 40$) compared with female controls ($n = 50$; threshold $P < 0.05$, corrected); and (b) female postmenopausal patients ($n = 20$) compared with female premenopausal patients ($n = 20$; threshold $P < 0.001$, uncorrected). (c) VBM analysis of T contrasts showing the negative correlation between gray matter volume and the period of time after menopause in female postmenopausal patients ($n = 20$; threshold $P < 0.001$, uncorrected).

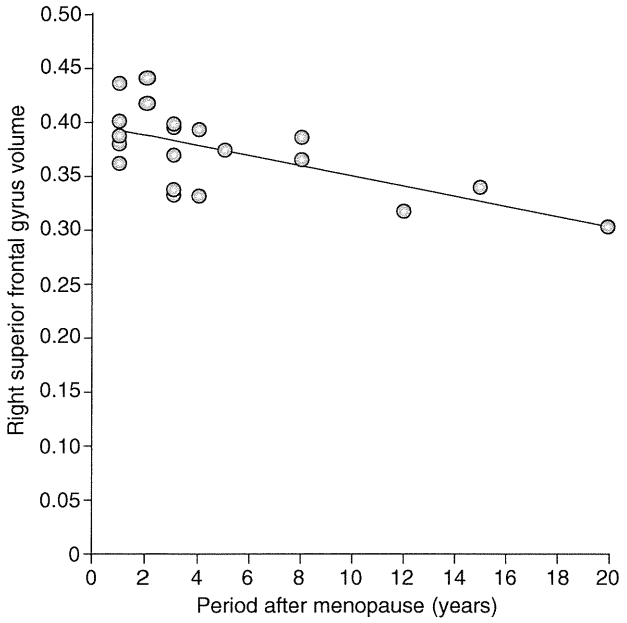

Figure 2. Correlation between gray matter volume of the right superior frontal gyrus and the period of time after menopause in female postmenopausal patients ($n = 20$).

the volume deficit in this region ($P < 0.001$ uncorrected). There was no significant correlation between longer postmenopausal interval and less volume deficit.

DISCUSSION

As a first step, we examined regional GM changes in female schizophrenia patients in relation to healthy female subjects by conducting VBM. The regions with remarkable GM volume reduction in patients were the insula, superior temporal gyrus, anterior cingulate, parahippocampal gyrus, and thalamus. The changes were predominantly found on the left side.

A meta-analysis reviewing 31 studies of VBM for GM volume in schizophrenia showed that patients had reduced GM density relative to control subjects in the bilateral insula, anterior cingulate, left postcentral gyrus, left parahippocampal gyrus, left middle frontal gyrus, and thalamus.[28] Another meta-analysis reviewed 15 studies of VBM for GM and WM volume in schizophrenia,[29] reporting that the areas significantly reduced in schizophrenia patients in >50% of the studies were the bilateral superior temporal gyrus, left medial frontal gyrus, left inferior frontal gyrus, and left parahippocampal gyrus.[29]

These two meta-analyses identified the morphology trait of schizophrenia using VBM. Generally, the present findings regarding patients versus controls are consistent with those of these meta-analyses in terms of locations and laterality.

We then examined the GM volume difference between postmenopausal patients and premenopausal patients. Direct comparison between the patient groups indicated morphological change in the left middle frontal gyrus. In addition, a significant correlation between brain morphology and interval after menopause was found in the right superior frontal gyrus. These regions are not identical, but both are located in the prefrontal area.

Volume reduction in the prefrontal area in schizophrenia patients has been observed in past studies, and morphological change in the prefrontal area has been indicated in relation to negative symptoms and cognitive impairment.[30] Additionally, a study regarding the relationship between illness duration and brain volume indicated that the right middle frontal cortex is particularly vulnerable to the long-term effect of schizophrenia.[16] According to these reports, the present results may indicate that postmenopausal patients are at a more advanced stage of progression.

A study on gender differences of brain morphology in schizophrenia reported that GM reductions in prefrontal areas were found predominantly in male patients.[9] It may be assumed that the duration of the low estrogen condition played a role in the morphological change in this area.

In the studies on menopause age of healthy subjects, the estimated median age at last menstruation period lies between 50 and 52 years.[31–33] A cross-sectional study concerning natural menopause of Japanese women reported that the median age of menopause was 50.54 years.[34]

The age of menopause of the postmenopausal patients in the present study, 41.8 ± 9.0 years, seemed considerably earlier than that of the healthy subjects. A major reason for this might be an antipsychotic medication-induced side-effect. Because of the very early age at menopause, the postmenopausal patient group in this study may not be a representative sample. This is a limitation of the study.

A study concerning the effect of antipsychotic-induced hyperprolactinemia in schizophrenia patients on antipsychotic medication showed that there was a significant inverse relationship between the prolactin levels in female patients and estradiol

levels, and when female patients with hyperprolactinemia were compared to those with a normal range of prolactin, only estradiol levels were significantly different between the two groups with regard to measured hormone levels (estradiol, testosterone, progesterone, luteinizing hormone, follicle-stimulating hormone, and thyroid-stimulating hormone).[35]

According to that study, it could be assumed that the young patients in the postmenopausal group with probable hyperprolactinemia had low estrogen levels in the present study. The gradual decline of ovarian estrogen production begins in the years prior to menopause, although a dramatic decline in plasma estrogen level occurs at the final menstrual cycle.[36] Research concerning gender differences and age of onset in schizophrenia has shown a second peak of onset in female patients in the age range 45–54 years, and it was hypothesized that the vulnerability threshold for schizophrenia is raised in women until menopause due to the effect of estrogen.[37] Therefore, a gradual loss of the protective role of estrogen against brain morphological change may also begin prior to menopause.

In healthy subjects, according to studies investigating the effect of estrogen on brain morphology in postmenopausal women, some reported adverse effects of hormone therapy associated with greater atrophy in the hippocampal region[38] or in the putamen,[39] while several others demonstrated that estrogen therapy slows age-related GM loss in frontal cortices,[11,13] temporal, parietal, and occipital cortices,[11] cerebellum,[11,13] and the hippocampal region,[11,12] findings partially in agreement with the present ones. Therefore, it is suggested that the effect of menopause on brain structural changes in schizophrenia patients could be attributable to the loss of the protective effect of estrogen against the pathophysiology of schizophrenia.

A limitation of the present study is that blood concentrations of sex hormones were not measured. Therefore, the present results do not represent the effects of sex hormones but rather the effects of menopause. In addition, because neither hormone levels nor menstrual state were checked in the healthy controls, the main purpose the patients versus controls analysis was to demonstrate that the overall tendency of the present patients would reflect the previous studies concerning the brain morphology of schizophrenia.

In conclusion, volumetric comparisons showed differential morphological alterations due to female hormonal change in schizophrenia. Postmenopausal patients had more GM volume reduction than premenopausal patients at the left middle frontal gyrus. In addition, there was significant correlation between brain morphology and interval after menopause in the right superior frontal gyrus. These results support the hypothesis of the protective role of estrogen against schizophrenia.

ACKNOWLEDGMENTS

Professor Hidenori Suzuki of the Department of Pharmacology, Nippon Medical School and Noriaki Yahata, PhD of the Department of Neuropsychiatry, Graduate School of Medicine, University of Tokyo are gratefully acknowledged. This study was supported by a Grant-in-Aid for Scientific Research from the Japanese Ministry of Education, Culture, Sports, Science and Technology (19390308), and a Health and Labor Sciences Research Grant for Research on Psychiatric and Neurological Diseases and Mental Health (H22-seishin-ippan-002) from the Japanese Ministry of Health, Labor and Welfare. All authors have no conflicts of interest.

REFERENCES

1. Seeman MV. Interaction of sex, age, and neuroleptic dose. *Compr. Psychiatry* 1983; 24: 125–128.
2. Bardenstein KK, McGlashan TH. Gender differences in affective, schizoaffective, and schizophrenic disorders. A review. *Schizophr. Res.* 1990; 3: 159–172.
3. Hafner H, Riecher A, Maurer K, Loffler W, Munk-Jorgensen P, Stromgren E. How does gender influence age at first hospitalization for schizophrenia? A transnational case register study. *Psychol. Med.* 1989; 19: 903–918.
4. Castle DJ, Murray RM. The epidemiology of late-onset schizophrenia. *Schizophr. Bull.* 1993; 19: 691–700.
5. Grigoriadis S, Seeman MV. The role of estrogen in schizophrenia: Implications for schizophrenia practice guidelines for women. *Can. J. Psychiatry* 2002; 47: 437–442.
6. Nopoulos P, Flaum M, Andreasen NC. Sex differences in brain morphology in schizophrenia. *Am. J. Psychiatry* 1997; 154: 1648–1654.
7. Gur RE, Turetsky BI, Cowell PE *et al.* Temporolimbic volume reductions in schizophrenia. *Arch. Gen. Psychiatry* 2000; 57: 769–775.
8. Job DE, Whalley HC, McConnell S, Glabus M, Johnstone EC, Lawrie SM. Structural gray matter differences between

first-episode schizophrenics and normal controls using voxel-based morphometry. *Neuroimage* 2002; **17**: 880–889.
9. Suzuki M, Nohara S, Hagino H *et al.* Regional changes in brain gray and white matter in patients with schizophrenia demonstrated with voxel-based analysis of MRI. *Schizophr. Res.* 2002; **55**: 41–54.
10. Bryant NL, Buchanan RW, Vladar K, Breier A, Rothman M. Gender differences in temporal lobe structures of patients with schizophrenia: A volumetric MRI study. *Am. J. Psychiatry* 1999; **156**: 603–609.
11. Boccardi M, Ghidoni R, Govoni S *et al.* Effects of hormone therapy on brain morphology of healthy postmenopausal women: A voxel-based morphometry study. *Menopause* 2006; **13**: 584–591.
12. Lord C, Buss C, Lupien SJ, Pruessner JC. Hippocampal volumes are larger in postmenopausal women using estrogen therapy compared to past users, never users and men: A possible window of opportunity effect. *Neurobiol. Aging* 2008; **29**: 95–101.
13. Robertson D, Craig M, van Amelsvoort T *et al.* Effects of estrogen therapy on age-related differences in gray matter concentration. *Climacteric* 2009; **12**: 301–309.
14. Ashburner J, Friston KJ. Voxel-based morphometry: The methods. *Neuroimage* 2000; **11**: 805–821.
15. Koutsouleris N, Gaser C, Jager M *et al.* Structural correlates of psychopathological symptom dimensions in schizophrenia: A voxel-based morphometric study. *Neuroimage* 2008; **39**: 1600–1612.
16. Premkumar P, Fannon D, Kuipers E, Cooke MA, Simmons A, Kumari V. Association between a longer duration of illness, age and lower frontal lobe grey matter volume in schizophrenia. *Behav. Brain Res.* 2008; **193**: 132–139.
17. McClure RK, Phillips I, Jazayerli R, Barnett A, Coppola R, Weinberger DR. Regional change in brain morphometry in schizophrenia associated with antipsychotic treatment. *Psychiatry Res.* 2006; **148**: 121–132.
18. Treloar AE. Menarche, menopause, and intervening fecundability. *Hum. Biol.* 1974; **46**: 89–107.
19. Overall JE, Brown WL. A factor analysis of several measures of choice behavior from a probability learning situation. *J. Gen. Psychol.* 1962; **66**: 115–128.
20. Faustmann PM, Ganz RE. Central cardio-autonomic disorganization in interictal states of epilepsy detected by phase space analysis. *Int. J. Neurosci.* 1994; **78**: 43–47.
21. Thiemann S, Csernansky JG, Berger PA. Rating scales in research: The case of negative symptoms. *Psychiatry Res.* 1987; **20**: 47–55.
22. Good CD, Johnsrude IS, Ashburner J, Henson RN, Friston KJ, Frackowiak RS. A voxel-based morphometric study of ageing in 465 normal adult human brains. *Neuroimage* 2001; **14**: 21–36.
23. Friston KJ, Tononi G, Reeke GN Jr, Sporns O, Edelman GM. Value-dependent selection in the brain: Simulation in a synthetic neural model. *Neuroscience* 1994; **59**: 229–243.
24. Friston KJ, Frith CD, Liddle PF, Dolan RJ, Lammertsma AA, Frackowiak RS. The relationship between global and local changes in PET scans. *J. Cereb. Blood Flow Metab.* 1990; **10**: 458–466.
25. Brett M, Johnsrude IS, Owen AM. The problem of functional localization in the human brain. *Nat. Rev. Neurosci.* 2002; **3**: 243–249.
26. Rey M, Dellatolas G, Bancaud J, Talairach J. Hemispheric lateralization of motor and speech functions after early brain lesion: Study of 73 epileptic patients with intracarotid amytal test. *Neuropsychologia* 1988; **26**: 167–172.
27. Lancaster JL, Woldorff MG, Parsons LM *et al.* Automated Talairach atlas labels for functional brain mapping. *Hum. Brain Mapp.* 2000; **10**: 120–131.
28. Glahn DC, Laird AR, Ellison-Wright I *et al.* Meta-analysis of gray matter anomalies in schizophrenia: Application of anatomic likelihood estimation and network analysis. *Biol. Psychiatry* 2008; **64**: 774–781.
29. Honea R, Crow TJ, Passingham D, Mackay CE. Regional deficits in brain volume in schizophrenia: A meta-analysis of voxel-based morphometry studies. *Am. J. Psychiatry* 2005; **162**: 2233–2245.
30. Goldman-Rakic PS, Selemon LD. Functional and anatomical aspects of prefrontal pathology in schizophrenia. *Schizophr. Bull.* 1997; **23**: 437–458.
31. Boldsen JL, Jeune B. Distribution of age at menopause in two Danish samples. *Hum. Biol.* 1990; **62**: 291–300.
32. McKinlay SM, Bifano NL, McKinlay JB. Smoking and age at menopause in women. *Ann. Intern. Med.* 1985; **103**: 350–356.
33. Brambilla DJ, McKinlay SM. A prospective study of factors affecting age at menopause. *J. Clin. Epidemiol.* 1989; **42**: 1031–1039.
34. Tamada T, Iwasaki H. [Age at natural menopause in Japanese women.] *Nihon. Sanka Fujinka Gakkai Zasshi* 1995; **47**: 947–952.
35. Smith S, Wheeler MJ, Murray R, O'Keane V. The effects of antipsychotic-induced hyperprolactinaemia on the hypothalamic-pituitary-gonadal axis. *J. Clin. Psychopharmacol.* 2002; **22**: 109–114.
36. Al-Azzawi F, Palacios S. Hormonal changes during menopause. *Maturitas* 2009; **63**: 135–137.
37. Hafner H, der Heiden W, Hambrecht M *et al.* [A chapter in systematic schizophrenia research: The search for causal explanations for sex differences in age of onset.] *Nervenarzt* 1993; **64**: 706–716.
38. Resnick SM, Espeland MA, Jaramillo SA *et al.* Postmenopausal hormone therapy and regional brain volumes: The WHIMS-MRI Study. *Neurology* 2009; **72**: 135–142.
39. Greenberg DL, Payne ME, MacFall JR, Provenzale JM, Steffens DC, Krishnan RR. Differences in brain volumes among males and female hormone-therapy users and nonusers. *Psychiatry Res.* 2006; **147**: 127–134.

Quantification of Dopamine Transporter in Human Brain Using PET with ^{18}F-FE-PE2I

Takeshi Sasaki[1,2], Hiroshi Ito[1,3], Yasuyuki Kimura[1], Ryosuke Arakawa[1], Harumasa Takano[1], Chie Seki[3], Fumitoshi Kodaka[1], Saori Fujie[1], Keisuke Takahata[1], Tsuyoshi Nogami[1], Masayuki Suzuki[1], Hironobu Fujiwara[1], Hidehiko Takahashi[1], Ryuji Nakao[4], Toshimitsu Fukumura[5], Andrea Varrone[4], Christer Halldin[4], Toru Nishikawa[2], and Tetsuya Suhara[1]

[1]Molecular Neuroimaging Program, Molecular Imaging Center, National Institute of Radiological Sciences, Chiba, Japan; [2]Department of Psychiatry and Behavioral Sciences, Tokyo Medical and Dental University Graduate School, Tokyo, Japan; [3]Biophysics Program, Molecular Imaging Center, National Institute of Radiological Sciences, Chiba, Japan; [4]Karolinska Institutet, Department of Clinical Neuroscience, Centre for Psychiatry Research, Karolinska Hospital, Stockholm, Sweden; and [5]Molecular Probe Program, Molecular Imaging Center, National Institute of Radiological Sciences, Chiba, Japan

^{18}F-(*E*)-*N*-(3-iodoprop-2*E*-enyl)-2β-carbofluoroethoxy-3β-(4-methylphenyl)nortropane (^{18}F-FE-PE2I) is a new PET radioligand with a high affinity and selectivity for the dopamine transporter (DAT). In nonhuman primates, ^{18}F-FE-PE2I showed faster kinetics and less production of radiometabolites that could potentially permeate the blood–brain barrier than did ^{11}C-PE2I. The aims of this study were to examine the quantification of DAT using ^{18}F-FE-PE2I and to assess the effect of radiometabolites of ^{18}F-FE-PE2I on the quantification in healthy humans. **Methods:** A 90-min dynamic PET scan was obtained for 10 healthy men after intravenous injection of ^{18}F-FE-PE2I. Kinetic compartment model analysis with a metabolite-corrected arterial input function was performed. The effect of radiometabolites on the quantification was evaluated by time-stability analyses. The simplified reference tissue model (SRTM) method with the cerebellum as a reference region was evaluated as a noninvasive method of quantification. **Results:** After the injection of ^{18}F-FE-PE2I, the whole-brain radioactivity showed a high peak (~3–5 standardized uptake value) and fast washout. The radioactive uptake of ^{18}F-FE-PE2I in the brain was according to the relative density of the DAT (striatum > midbrain > thalamus). The cerebellum showed the lowest uptake. Tissue time–activity curves were well described by the 2-tissue-compartment model (TCM), as compared with the 1-TCM, for all subjects in all regions. Time stability analysis showed stable estimation of total distribution volume with 60-min or longer scan durations, indicating the small effect of radiometabolites. Binding potentials in the striatum and midbrain were well estimated by the SRTM method, with modest intersubject variability. Although the SRTM method yielded a slight underestimation and overestimation in regions with high and low DAT densities, respectively, binding potentials by the SRTM method were well correlated to the estimates by the indirect kinetic method with 2-TCM. **Conclusion:** ^{18}F-FE-PE2I is a promising PET radioligand for quantifying DAT. The binding potentials could be reliably estimated in both the striatum and midbrain using both the indirect kinetic and SRTM methods with a scan duration of 60 min. Although radiometabolites of ^{18}F-FE-PE2I in plasma possibly introduced some effects on the radioactivity in the brain, the effects on estimated binding potential were likely to be small.

Key Words: ^{18}F-FE-PE2I; positron emission tomography; dopamine transporter; kinetic modeling; radiometabolite

J Nucl Med 2012; 53:1065–1073
DOI: 10.2967/jnumed.111.101626

Dopamine transporter (DAT) plays a crucial role in the regulation of dopamine concentration in the synaptic cleft by dopamine reuptake. Changes in the density and function of DAT have been reported in various neuropsychiatric disorders, such as Parkinson disease (*1*), Huntington disease (*2*), attention-deficit/hyperactivity disorder (*3*), autism (*4*), and schizophrenia (*5*). Although DAT ligands for SPECT have been widely used in clinical practice, developing a useful radioligand for PET—which has higher resolution and better ability of quantification than SPECT—is the key to assessing its role in the pathophysiology of these diseases and to developing new therapeutic approaches for them.

Several radioligands for imaging DAT have been developed and used for PET. Among ^{11}C-labeled radioligands, ^{11}C-cocaine (*6*), ^{11}C-WIN35,428 (CFT) (*7*), ^{11}C-β-CIT (*8*), and ^{11}C-DL-threo-methylphenidate (*9*) have relatively low affinity for DAT or have slow kinetics in the high-DAT-density regions. ^{11}C-altropane has high affinity and selectivity for DAT (*10*), but the kinetics in the human brain have not been reported in detail to our knowledge. The ^{18}F-labeled radioligands that have been studied in humans so far include ^{18}F-CFT (^{18}F-WIN35,428) (*11*), *N*-3-fluoropropyl-2-β-carboxymethoxy-3-β-(4-iodophenyl)

Received Dec. 6, 2011; revision accepted Feb. 27, 2012.
For correspondence or reprints contact: Hitoshi Ito, Biophysics Program, Molecular Imaging Center, National Institute of Radiological Sciences, 4-9-1, Anagawa, Inage-ku, Chiba, 263-8555, Japan.
E-mail: hito@nirs.go.jp
Published online Jun. 11, 2012.

nortropane (^{18}F-FPCIT) (*12*), and 2β-carbomethoxy-3β-(4-chlorophenyl)-8-(2-fluoroethyl)nortropane (^{18}F-FECNT) (*13*). All of them have high affinity and selectivity for DAT, but the kinetics are relatively slow, and more than 90 min are needed to reach peak uptake in the striatum.

Recently, a new ligand, *N*-(3-iodoprop-2*E*-enyl)-2β-carbomethoxy-3β-(4-methylphenyl)nortropane (PE2I), with a high affinity for DAT (inhibition constant, 17 nM) and good selectivity, was developed (*14,15*). In human PET studies, ^{11}C-PE2I showed a high specific-to-nonspecific ratio (*15–18*). However, 2 problems have been reported in quantifying DAT with ^{11}C-PE2I. First, because of the relatively slow kinetics of ^{11}C-PE2I in the striatum, reference tissue methods severely (~50%) underestimated DAT binding in this region, compared with those by the methods with arterial input function (*16,17*). Second, a radiometabolite of ^{11}C-PE2I has been found to cross the blood–brain barrier (BBB) in rats, thus potentially reducing the accuracy of the quantification of DAT (*19*).

A fluoroethyl analog of PE2I, ^{18}F-(*E*)-*N*-(3-iodoprop-2*E*-enyl)-2β-carbofluoroethoxy-3β-(4-methylphenyl)nortropane (^{18}F-FE-PE2I) (inhibition constant, 12 nM), has recently been developed and evaluated in nonhuman primates (*20*). In monkeys, ^{18}F-FE-PE2I was more favorable for the quantitative analysis of DAT, because it showed faster kinetics and less production of BBB-permeable radiometabolites than did ^{11}C-PE2I. The quantification of DAT with ^{18}F-FE-PE2I was less biased than that with ^{11}C-PE2I (*21*).

The aims of this study were to examine the method for quantification of DAT using ^{18}F-FE-PE2I and to assess the effect of radiometabolites of ^{18}F-FE-PE2I on the quantification in healthy humans.

MATERIALS AND METHODS

Subjects

Ten healthy men (mean age ± SD, 28.1 ± 6.9 y; age range, 20–39 y) participated in this study. All subjects were free of any somatic, neurologic, or psychiatric disorders. The study was approved by the Ethics and Radiation Safety Committee of the National Institute of Radiologic Sciences, Chiba, Japan. Written informed consent was obtained from all subjects before their inclusion in the study.

PET Procedure

^{18}F-FE-PE2I was synthesized from its acid precursor through a reaction with ^{18}F-2-bromo-1-fluoroethane in dimethylformamide and sodium hydroxide in *N,N*-dimethylformamide, as previously described (*22*).

A 90-min dynamic scan was obtained for each subject after a 1-min intravenous injection of ^{18}F-FE-PE2I using a PET scanner system (ECAT EXACT HR+; CTI-Siemens) The scan protocol consisted of 9 frames of 20 s, 5 frames of 1 min, 4 frames of 2 min, 12 frames of 4 min, and 5 frames of 6 min. The injected dose and specific activity were 183.0 ± 9.3 MBq and 146.1 ± 98.7 GBq/μmol at the time of injection, respectively. A head holder was used to minimize head movements. Scatter correction was performed. Attenuation correction was based on a transmission scan using a $^{68/68}$Ge/Ga source.

Arterial Blood Sampling and Metabolite Analysis

Arterial blood samples were taken manually 32 times after the injection of radioligand to obtain an arterial input function. Each blood sample was centrifuged to obtain plasma and blood cell fractions, and the concentration of radioactivity in whole blood and plasma was measured.

The fractions of the parent and its radiometabolites in plasma were determined by high-performance liquid chromatography (HPLC) from 10 blood samples for each subject. Each plasma sample had acetonitrile added and then was centrifuged. The supernatant of the centrifuged sample was subjected to radio-HPLC analysis (column, μBondapak C18 [Waters]). Acetonitrile (90%) (A) and phosphoric acid (0.01 M) (B) were used as mobile phases, with a flow rate of 6.0 mL/min. Gradient elution was used with the following gradient profile: 0–4.5 min, 25/75–70/30 A/B; 4.5–8.0 min, 70/30–25/75 A/B; and 8.0–10.0 min, 25/75–25/75 A/B. Linear interpolation was used to calculate the fractions of the parent and radiometabolites for the blood samples without metabolite analysis.

Image Analysis

T1-weighted MR images acquired with a 1.5-T MRI scanner (Gyroscan NT; Philips) (1-mm-slice axial images; repetition time, 21 ms; echo time, 9.2 ms; and flip angle, 30°) were coregistered to the corresponding PET images. Manually drawn volumes of interest were based on the anatomic information of MR images. Then, these volumes of interest were applied to the dynamic PET images to extract time–activity curves for the putamen, caudate, ventral midbrain (including the substantia nigra and ventral tegmental area), thalamus, and cerebellum. All image and kinetic analyses were performed using PMOD (version 3.0; PMOD Technologies).

Kinetic Analysis

Standard 1- and 2-tissue-compartment models (TCMs) (*18,23*) with an arterial input function (concentration of the parent in plasma) were used to estimate rate constants and total distribution volume (V_T) by an iterative nonlinear least-squares curve-fitting procedure without weighting. Linear interpolation was used to calculate the concentration of the parent in plasma at the time points of time–activity curves of tissue. The rate constants K_1 and k_2 represent the influx and efflux rates, respectively, for radioligand diffusion across the BBB. For 2-TCM, the rate constants k_3 and k_4 represent radioligand transfer between the compartments for nondisplaceable and specifically bound radioligand, respectively. V_T is equal to the ratio of the concentration of radioligand in tissue to that in plasma at equilibrium. Blood volume was fixed at 0.05 mL/mL (*24*). The binding potential (BP_{ND}) of ^{18}F-FE-PE2I was quantified by the indirect kinetic method. We used the cerebellum as the reference brain region because of its negligible DAT density as shown in a human autoradiographic study (*25*) and an in vivo displacement study in monkeys (*20*). BP_{ND} can be expressed as:

$$BP_{ND} = \left(V_{T(regions)}/V_{T(cerebellum)}\right) - 1,$$

where $V_{T(regions)}$ and $V_{T(cerebellum)}$ are V_T of target regions and the cerebellum, respectively.

Time–Stability Analysis

To investigate the effect of scan length on the estimation of V_T, we analyzed PET data while truncating scan length. The scan length from 90 to 40 min, with 10-min decrements, was analyzed to estimate V_T of varying scan lengths, using the parent concentration in plasma as the input function. For each region and duration,

V_T was expressed as the percentage of the V_T value obtained with a 90-min scan length.

Kinetic Analysis with Radiometabolite-Included Input Function

To assess the effect of lipophilic radiometabolites, we tested an alternative input function consisting of the concentration of the parent and the lipophilic radiometabolite, 4-hydroxymethyl analog of the parent (M1), to estimate rate constants and V_T.

Simplified Reference Tissue Model (SRTM)

^{18}F-FE-PE2I binding was also quantified by the SRTM method with the cerebellum as a reference region. Assuming that both target and reference regions have the same level of nondisplaceable binding, and the kinetics in the target and reference regions can be described by 1-TCM, BP_{ND} is obtained by solving the convolution equation using a nonlinear least-squares fitting procedure (*26*). In this method, the parameters are reduced to 3: R_1 (ratio of K_1 relative to the reference region), k_2, and BP_{ND}. In addition, to investigate the applicability of shorter study durations, BP_{ND} values estimated by the indirect kinetic method and by the SRTM method with 60-min scanning data were compared with those estimated with 90-min scanning data.

Statistical Analysis

The goodness of curve fitting of models with different levels of complexity was compared using the Akaike information criterion (AIC) (*27*) and F test. In a model with better fitting, AIC shows lower values. A P value of less than 0.05 was considered significant for the F test. The SE of kinetic parameters was given by the diagonal of the covariate matrix (*28*). Divided by the estimate of the parameter itself, SE was expressed as a percentage (SE/[estimates of the parameter]) and used to assess parameter identifiability. A smaller percentage indicates better identifiability. Pearson r and linear regression analyses were used to assess correlations between BP_{ND} values estimated with the different approaches. A paired t test was applied to assess the difference in BP_{ND} values between the indirect kinetic and SRTM methods.

RESULTS

Brain Uptake

After the injection of ^{18}F-FE-PE2I, the radioactivity was distributed throughout the brain, with a high peak (~3–5 SUV) and fast washout (Figs. 1 and 2A). The peak uptake occurred within 10 min in all regions. The rank order of radioactivity from approximately 15 min to the end of the scan was as follows: putamen and caudate >> midbrain > thalamus > cerebellum. The uptake in the midbrain was visible as 2 distinct regions. Specific binding, which is the difference in radioactivity between target regions and the cerebellum, reached peak levels within approximately 30 min after injection in all target regions (Fig. 2B). The ratio of radioactivity in the striatum to that in the cerebellum reached a peak level (~7.0) approximately 60 min after the injection and remained at almost the same level thereafter (Fig. 2C).

Plasma Analysis

Reversed-phase HPLC analysis of plasma resulted in the separation of the parent and 2 major radiolabeled components (Fig. 3A). The peak with longest retention time corresponded to the parent, representing approximately 14% of plasma radioactivity at 30 min after injection (Fig. 3B). Of the 2 major radiolabeled components, one (M1) was retained longer, representing approximately 20% of plasma radioactivity at 30 min after injection. The M1-to-parent ratio was stable (~1.3–1.4) at 20 min after injection. Retention of the other one (M2) was shorter and consisted of 2 peaks, which were not sufficiently separated from each other, representing approximately 70% of the plasma radioactivity at 30 min after injection. The concentration of the parent showed a quick peak and fast washout in plasma (Fig. 3C).

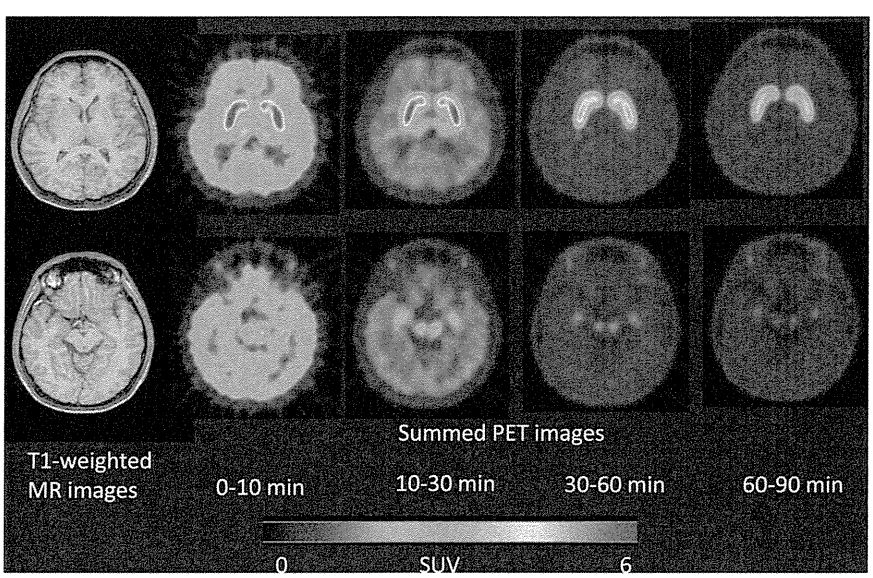

FIGURE 1. Representative dynamic PET images of healthy subject injected with ^{18}F-FE-PE2I. PET images were created at level of striatum (top) and midbrain (bottom). SUV = standardized uptake value.

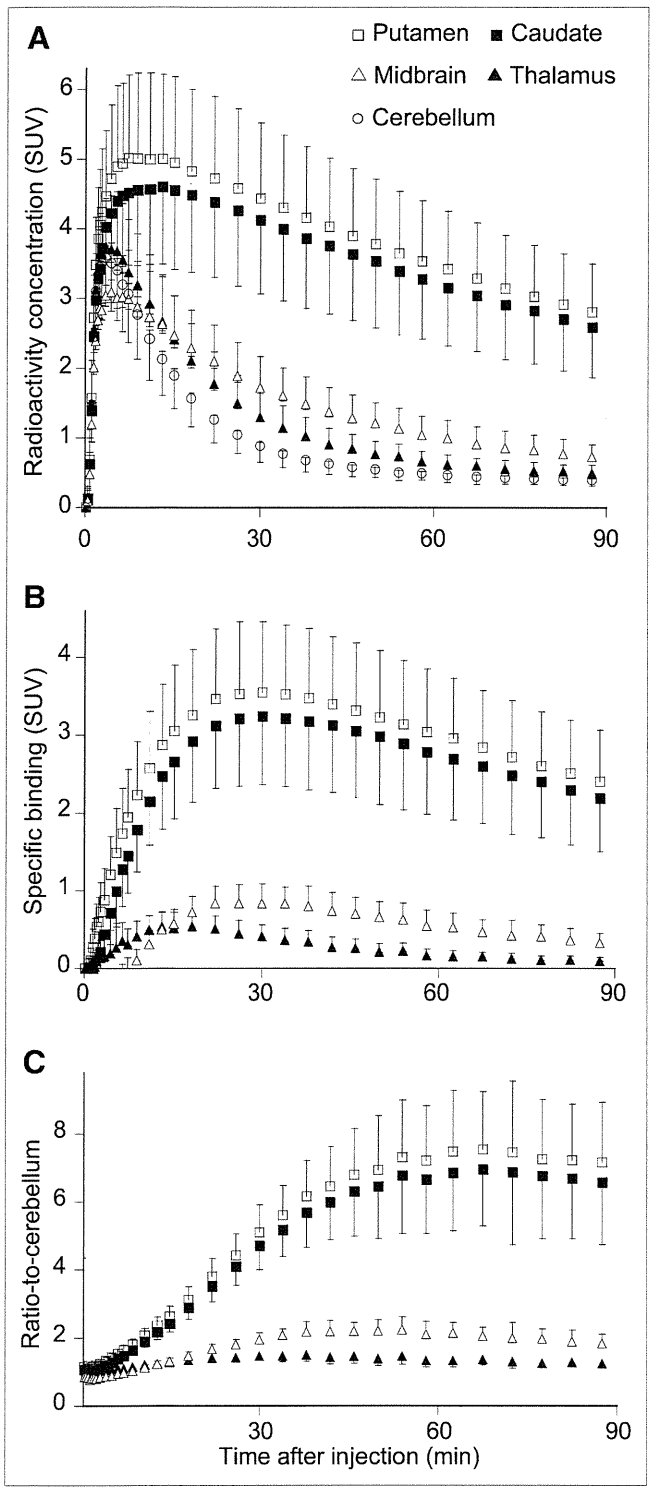

FIGURE 2. Average time course of radioactivity in brain regions after injection of ^{18}F-FE-PE2I. Time course for regional radioactivity (A), specific binding (B), and ratio to cerebellum (C). Data represent mean ± SD of all 10 subjects. SUV = standardized uptake value.

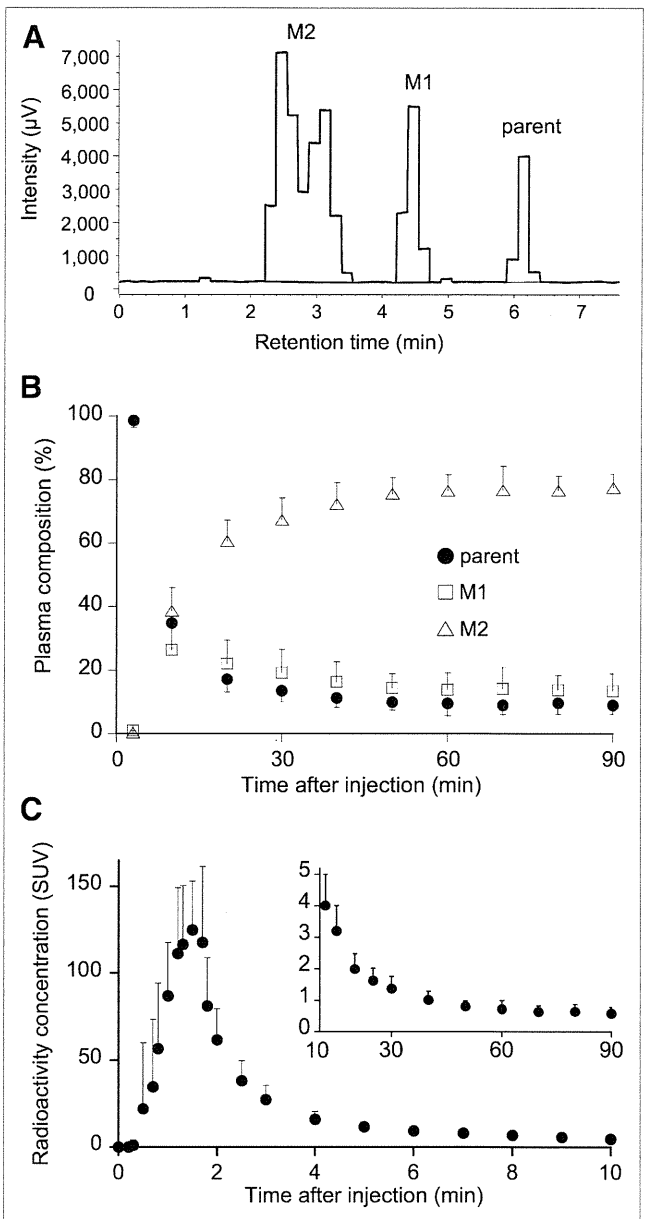

FIGURE 3. Concentration of ^{18}F-FE-PE2I and its composition in arterial plasma after injection of ^{18}F-FE-PE2I. (A) Representative radiochromatogram at 30 min after injection of ^{18}F-FE-PE2I. (B) Plasma composition of parent, M1, and M2. (C) Concentration of ^{18}F-FE-PE2I in plasma. Values from 0 to 10 and 10 to 90 min are shown in each graph with different ranges of *y*-axis. Data represent mean ± SD of all 10 subjects. SUV = standardized uptake value.

Quantification of DAT by Compartment Analysis

The 2-TCM provided significantly better fitting than the 1-TCM for all subjects in all regions. AIC of the 2-TCM was significantly lower than that of the 1-TCM in all regions in all subjects (paired *t* test, $P < 0.05$). The *F* test showed that the 2-TCM gave statistically better fittings than did the 1-TCM in all regions in all subjects ($F > 10.2$, $P < 0.001$). Thus, time–activity curves of all regions including the cerebellum were better described by the 2-TCM (Fig. 4).

The 2-TCM estimated K_1 and V_T with good identifiability (1.8% and 3.7%, respectively) (Table 1). BP_{ND} values estimated by the indirect kinetic method were approximately 4.0–4.5 in the putamen and caudate, approximately 0.5 in

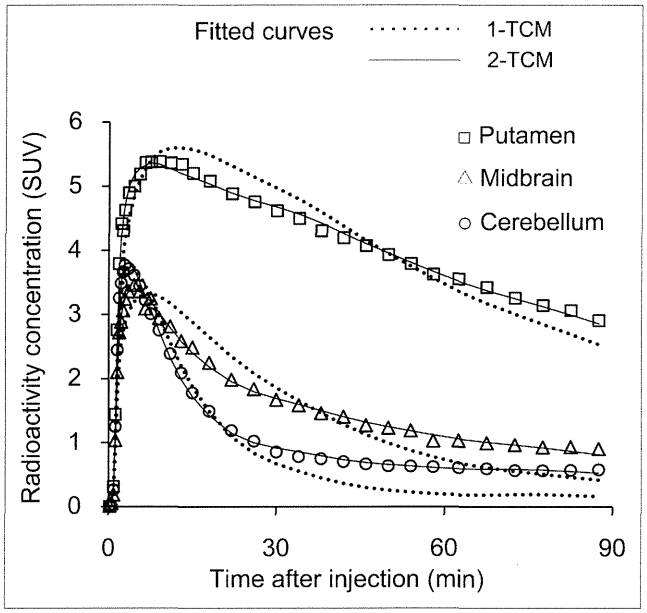

FIGURE 4. Representative fitted model curves of 1-TCM and 2-TCM. Time–activity curves in putamen, midbrain, and cerebellum were fitted to 1-TCM and 2-TCM using parent in plasma as input function. The 2-TCM (solid line) provided better fittings than 1-TCM (dotted line) for all 3 regions. SUV = standardized uptake value.

the midbrain, and approximately 0.2 in the thalamus (Table 2). As to the intersubject variability, the coefficients of variation (100 × SD/mean) of the BP_{ND} values were approximately 20%–25% in the putamen and caudate, approximately 30% in the midbrain, and approximately 60% in the thalamus.

Effects of Scan Length on Quantification of DAT

V_T values were stably estimated using the 2-TCM with 60-min or longer scan length. In the putamen and cerebellum, V_T values gradually increased with longer scan length (Figs. 5A and 5B). With a 60-min scan length, V_T values were approximately 94% and 90% of those with full scan length in the putamen and cerebellum, respectively, indicating that V_T values were stably estimated with a 60-min or longer scan length. Identifiability of V_T in the putamen improved over time, reaching approximately 2% at 90 min, whereas in the cerebellum, it remained at almost the same level (~6%) at a 60-min or longer scan length.

Effects of Adding Lipophilic Radiometabolite to Input Function on Quantification of DAT

To assess the effect of the lipophilic radiometabolite, we tested an alternative input function consisting of the concentration of the parent and M1, the lipophilic radiometabolite. Although the 2-TCM showed significantly better fitting than did the 1-TCM in the putamen, caudate, and midbrain based on AIC and the F test, V_T was not well identified by the 2-TCM in the thalamus in some subjects and in the cerebellum in most subjects. In the putamen, caudate, and midbrain, V_T values estimated using the alternative input function were approximately 30%–35% lower than V_T values estimated with the parent concentration in plasma as the input function (Supplemental Table 1; supplemental materials are available online only at http://jnm.snmjournals.org).

Quantification of DAT with SRTM Method

BP_{ND} values estimated by the SRTM method were approximately 3.6–4.0 in the putamen and caudate, approximately 0.6 in the midbrain, and approximately 0.3 in the thalamus (Table 2). Simple correlation analysis showed good correlation between BP_{ND} values estimated by the indirect kinetic method and by the SRTM method (r = 0.990, $P < 0.0001$) (Fig. 6), although there was significant difference between these values ($P = 0.0094$, paired t test). A Bland–Altman plot showed that the SRTM method underestimated BP_{ND} in the high-density regions and overestimated BP_{ND} in the low-density regions; however, the magnitude of the bias was small (~10% in the putamen, caudate, and midbrain) (Supplemental Fig. 1). The intersubject variability of BP_{ND} by the SRTM method was

TABLE 1
Kinetic Parameters by 2-TCM Using Parent as Input Function

Region	K_1 (mL·cm^{-3}·min^{-1})	k_2 (min^{-1})	k_3 (min^{-1})	k_4 (min^{-1})	K_1/k_2 (mL·cm^{-3})	k_3/k_4	V_T (mL·cm^{-3})	AIC
Putamen	0.292 ± 0.053 (1.7)	0.073 ± 0.022 (15)	0.133 ± 0.030 (21)	0.043 ± 0.007 (8.6)	4.25 ± 1.07 (13)	3.19 ± 0.97 (17)	17.3 ± 4.6 (2.0)	−43 ± 21
Caudate	0.248 ± 0.047 (1.7)	0.051 ± 0.022 (19)	0.110 ± 0.063 (38)	0.051 ± 0.014 (17)	5.71 ± 2.69 (18)	2.09 ± 0.93 (27)	16.2 ± 5.5 (2.6)	−38 ± 16
Midbrain	0.203 ± 0.044 (2.6)	0.095 ± 0.026 (13)	0.053 ± 0.028 (34)	0.042 ± 0.009 (22)	2.18 ± 0.37 (11)	1.29 ± 0.55 (18)	4.9 ± 1.1 (3.8)	20 ± 20
Thalamus	0.269 ± 0.042 (1.7)	0.123 ± 0.024 (6.0)	0.029 ± 0.018 (26)	0.041 ± 0.023 (23)	2.26 ± 0.55 (4.7)	0.71 ± 0.20 (12)	3.8 ± 0.8 (3.8)	10 ± 16
Cerebellum	0.265 ± 0.031 (1.2)	0.141 ± 0.025 (3.5)	0.013 ± 0.005 (23)	0.023 ± 0.013 (30)	1.94 ± 0.44 (2.6)	0.67 ± 0.32 (15)	3.2 ± 0.7 (6.3)	−4 ± 29

Values are mean ± SD (n = 10), with percentage SE (which is inversely related to identifiability of parameters) in parentheses.

TABLE 2
BP_{ND} Values by Indirect Kinetic and SRTM Methods

Region	BP_{ND}	
	Indirect kinetic	SRTM
Putamen	4.46 ± 0.95	4.05 ± 0.66
Caudate	4.06 ± 1.04	3.61 ± 0.67
Midbrain	0.55 ± 0.17	0.62 ± 0.13
Thalamus	0.20 ± 0.12	0.29 ± 0.08

Values are mean ± SD (n = 10).

approximately 15%–20% in the striatum and midbrain and approximately 30% in the thalamus, which were overall smaller than those by the indirect kinetic method. When BP_{ND} values estimated by the indirect kinetic method and by the SRTM method with 60-min data were compared with those estimated with 90-min data, good correlations were observed (r = 0.992 for the indirect kinetic method and 0.999 for the SRTM method, $P < 0.0001$ for both, Figs. 7A and 7B).

DISCUSSION

^{18}F-FE-PE2I is a promising radioligand for quantifying DAT in healthy humans. The kinetics of ^{18}F-FE-PE2I were well described by a standard 2-TCM using the parent radioligand in plasma as the input function. Although the radiometabolites of ^{18}F-FE-PE2I possibly have some effect on the radioactivity in the brain, the effect on the quantification was likely to be small. As a noninvasive quantification of DAT, the SRTM method was validated. The quantification was stable in both the striatum and the midbrain for both the indirect kinetic method with 2-TCM and the SRTM method with a scan duration of 60 min.

General kinetics of ^{18}F-FE-PE2I showed promising characteristics, including a high specific-to-nonspecific ratio and relatively fast washout. Uptake was high in the putamen and caudate, relatively low in the midbrain and thalamus, and lowest in the cerebellum. In all target regions, specific binding reached maximum values within the duration of PET data acquisition, and transient equilibrium was reached during this acquisition period. Uptake in the midbrain was visualized as 2 distinct regions. Given the selectivity of ^{18}F-FE-PE2I for DAT in the midbrain shown by a displacement study (*20*), we suppose that this uptake reflected DAT binding, not serotonin transporter binding.

Compartment model analysis showed that the kinetics of ^{18}F-FE-PE2I were well described by the 2-TCM using the parent radioligand in plasma as the input function. To estimate BP_{ND}, we applied the indirect kinetic method instead of directly using the ratio of k_3/k_4 values. The k_3/k_4 ratio theoretically equals BP_{ND}, but this estimate tends to be inaccurate because of data noise (*29*). We actually observed that these values showed poor identifiability and were not so reliably estimated (Table 1). Regional BP_{ND} values were

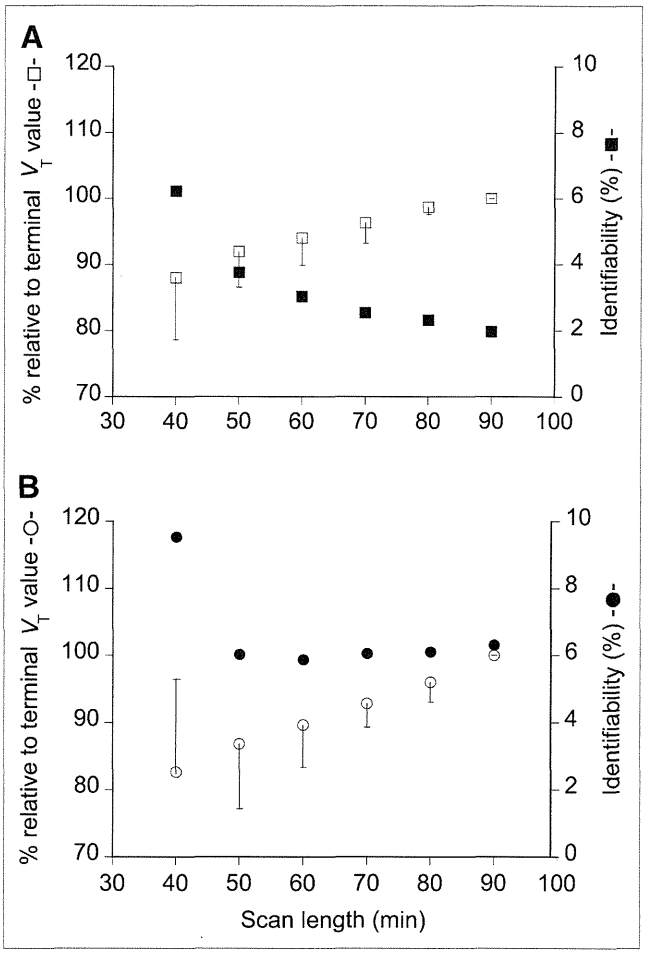

FIGURE 5. Value of V_T and identifiability as function of scan length. V_T and its corresponding SE (%) (SE (%)) were estimated in putamen (A) and cerebellum (B) with 2-TCM using parent as input function with truncating scan length from 90 to 40 min. V_T values are expressed as percentage of terminal value and plotted along left y-axis for putamen (□) and cerebellum (○). Corresponding SE (%), which is inversely related to identifiability, is plotted along right y-axis for putamen (■) and cerebellum (●). Error bar represents SD (n = 10).

in accordance with previous autoradiographic (*25*) and in vivo studies (*16,17*). As to intersubject variability, coefficients of variation of the BP_{ND} values were good in the putamen and caudate, acceptable in the midbrain, and poor in the thalamus. Because the BP_{ND} value in the midbrain was low (~13% of that in the striatum) in comparison with the results of autoradiography (~50% of that in the striatum) (*25*), the BP_{ND} values in the midbrain could be affected by the partial-volume effect. Similar results were obtained in nonhuman primates using high-resolution research tomography. BP_{ND} in the midbrain was approximately 15% of the values in the striatum (*21*).

Although radiometabolites of ^{18}F-FE-PE2I possibly have some effects on radioactivity in the brain, their effect on quantification was likely to be small. HPLC analysis detected 2 radiometabolites of ^{18}F-FE-PE2I in plasma,

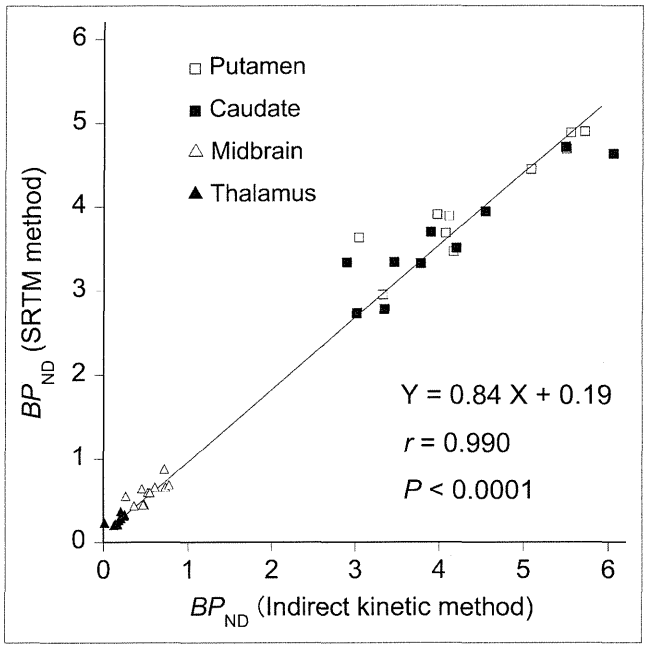

FIGURE 6. Correlation of BP_{ND} values estimated by indirect kinetic method using parent as input function and by SRTM method. BP_{ND} values showed significant correlation between 2 methods. Each data point represents BP_{ND} values in respective regions of each subject.

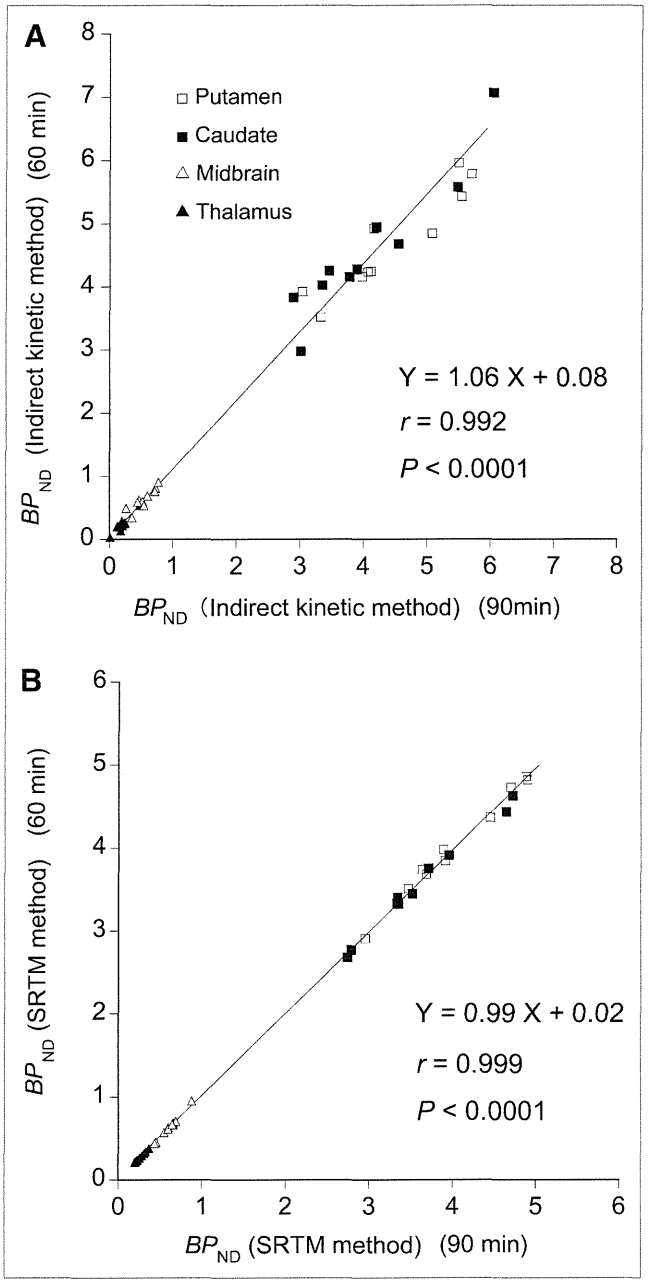

FIGURE 7. Correlation of BP_{ND} values estimated with 60- and 90-min data. (A) BP_{ND} values estimated by indirect kinetic method. (B) BP_{ND} values estimated by SRTM method. Significant correlations were observed in both methods between estimates with 60- and 90-min data.

one with intermediate (M1) and the other with lower (M2) lipophilicity. M1 and M2 would be 4-hydroxymethyl and 4-carboxyl analogs of ^{18}F-FE-PE2I, respectively, on the basis of the retention time of HPLC analysis, compared with the rat study (*19*). For clarity, in the following sentences, we refer to 4-hydroxymethyl and 4-carboxyl analogs of ^{11}C-PE2I as M1′ and M2′, respectively. In rats, M1′ entered the brain, accumulated in the striatum to a lesser extent than ^{11}C-PE2I, and metabolized to M2′, which accumulated in the brain. Mainly as a result of the accumulation of M2′, radioactivity in the cerebellum of rats did not decrease from 55 min to the end of the scan (120 min) (*19*). Whereas in the current study with ^{18}F-FE-PE2I, radioactivity in the cerebellum showed a gradual decrease to the end of the scan (90 min) (Fig. 2A), indicating that the amount of retention of radiometabolites in the brain in humans with ^{18}F-FE-PE2I was less than that in rats with ^{11}C-PE2I. This result was in accordance with the study in monkeys with ^{18}F-FE-PE2I (*21*).

The effects of radiometabolites on the quantification were small in the target and reference regions. To evaluate the effect of the possible accumulation of radiometabolites on the estimation of V_T, we performed a time–stability analysis of V_T. The increase in V_T with an increase in scan length could be interpreted as evidence for the accumulation of radiometabolites in the brain (*30*). In the current study, V_T values by the 2-TCM in the putamen and cerebellum with 60-min data were approximately 94% and 90% of terminal values with 90-min data (Fig. 6). This finding might indicate that V_T values were slightly affected by the radiometabolites, but the effects were relatively small.

To estimate the possible bias by the radiometabolites on V_T, we tried a combined input function of the parent and the radiometabolite M1 as previously performed by Varrone et al. in nonhuman primates using^{18} F-FE-PE2I (*21*). The main assumption of this approach is that the parent and the radiometabolite M1 would behave similarly and hence could be combined in a single input. With this approach,

the 2-TCM yielded approximately 30%–35% lower estimates of V_T values in the striatum and midbrain than with the 2-TCM using the parent as the input function. The decrease of V_T could be a possible maximum bias by the radiometabolites. However, the V_T values estimated by the 2-TCM using a summation of the parent and M1 as the input function were not well identified in some subjects in the thalamus and in most in the cerebellum. Because combining the parent and M1 as the input function did not improve the fitting, at least for these regions the assumption was not fully supported by the data. Identification of the radiometabolites of ^{18}F-FE-PE2I and assessment of their affinity for the DAT would be necessary to confirm or rule out the above assumption.

As a less noninvasive quantification of DAT without arterial blood data, BP_{ND} values were well estimated by the SRTM method using the cerebellum as the reference region. BP_{ND} values estimated by the SRTM method were well correlated with those estimated by the indirect kinetic method with the 2-TCM, which was not so much affected by radiometabolites as we discussed above. The SRTM method yielded slight underestimation and overestimation of BP_{ND} values in regions with high and low DAT densities, respectively, although the magnitude of the bias was small (~10% in the putamen, caudate, and midbrain). This bias seems to be an intrinsic limitation of the SRTM method because a similar phenomenon was observed in other ligands, including the serotonin 5-hydroxytryptamine-1A ligand ^{11}C-WAY-100653 (*31*), perhaps because of a violation of the assumptions of SRTM method. The intersubject variability of BP_{ND} values by the SRTM method were better than those by the indirect kinetic method with the 2-TCM, indicating that the SRTM method provided more precise estimation of BP_{ND} in all regions, including the midbrain.

Time–stability analysis indicated that 60-min scan duration is enough to estimate DAT binding with ^{18}F-FE-PE2I in humans. A recent study in nonhuman primates indicated that an approximately 60-min scan length was sufficient for the quantification of DAT with ^{18}F-FE-PE2I by the SRTM method (*32*). In the current study in humans, quantification was stable for both the indirect kinetic method and SRTM method with a scan duration of 60 min. Good correlations were observed between BP_{ND} values estimated with 60- and 90-min data for both the indirect kinetic method and the SRTM method.

^{18}F-FE-PE2I has many desirable characteristics among DAT ligands available for human imaging. High affinity and high selectivity for DAT allowed reliable quantification of specific binding not only in the striatum but also in the midbrain. Because of the faster kinetics even in high-density regions (i.e., the striatum), quantification with a shorter time (60 min) was possible, and the SRTM method yielded less biased BP_{ND} in the striatum than ^{11}C-PE2I. In addition, labeling with ^{18}F, which has a longer half-life than ^{11}C (110 vs. 20 min), allows distribution of the radioligand to PET centers without a cyclotron.

^{18}F-labeled DAT ligands previously reported in humans include ^{18}F-FPCIT (*12*), ^{18}F-CFT (^{18}F-WIN35,428) (*11*), and ^{18}F-FECNT (*13*). All of these ligands have a high affinity for DAT, and the maximum striatum-to-cerebellum ratios have been reported to be approximately 3.5–9.0. The possible advantage of ^{18}F-FPCIT and ^{18}F-FECNT could be the absence of potentially BBB-permeable radiometabolites. However, the disadvantage of those ligands was that the kinetics are slow, requiring over 90 min to reach peak brain uptake in the striatum. Among ^{18}F-labeled DAT ligands, ^{18}F-FE-PE2I has a relatively high striatum-to-cerebellum ratio (~7.0) and obviously the fastest kinetics.

One of the 2 limitations of the current study is the absence of the measurement of the free fraction in plasma, which would enable us to measure DAT density more accurately. Another limitation is the absence of an animal ex vivo study using ^{18}F-FE-PE2I to examine the BBB permeability and affinity for DAT of the radiometabolites. These issues should be explored in future studies.

CONCLUSION

^{18}F-FE-PE2I is a promising radioligand for quantifying DAT in healthy humans. The kinetics of ^{18}F-FE-PE2I were well described by a standard 2-TCM using the parent radioligand in plasma as the input function. Although radiometabolites of ^{18}F-FE-PE2I possibly have some effect on the radioactivity in the brain, their effect on quantification was likely to be small. As a noninvasive quantification of DAT, the SRTM method was validated. The quantification was stable in both the striatum and the midbrain for both the indirect kinetic method with 2-TCM and the SRTM method with a scan duration of 60 min, although the SRTM method yielded a slight underestimation and overestimation of BP_{ND} values in regions with high and low DAT densities, respectively. If no major differences in metabolism between patients and controls are present in clinical studies, noninvasive estimation of BP_{ND} by the SRTM method with a 60-min scan will be sufficiently accurate for DAT quantification.

DISCLOSURE STATEMENT

The costs of publication of this article were defrayed in part by the payment of page charges. Therefore, and solely to indicate this fact, this article is hereby marked "advertisement" in accordance with 18 USC section 1734.

ACKNOWLEDGMENTS

We thank Katsuyuki Tanimoto, Takahiro Shiraishi, and Takehito Ito for their assistance in performing PET experiments and Izumi Izumida and Kazuko Suzuki for their help as clinical research coordinators. This study was supported by a grant-in-aid for Molecular Imaging Program from the Ministry of Education, Culture, Sports, Science and Technology and by a Health Labour Sciences Research

grant from the Ministry of Health, Labour and Welfare, Japanese government. No other potential conflict of interest relevant to this article was reported.

REFERENCES

1. Hurley MJ, Mash DC, Jenner P. Markers for dopaminergic neurotransmission in the cerebellum in normal individuals and patients with Parkinson's disease examined by RT-PCR. *Eur J Neurosci.* 2003;18:2668–2672.
2. Ginovart N, Lundin A, Farde L, et al. PET study of the pre- and post-synaptic dopaminergic markers for the neurodegenerative process in Huntington's disease. *Brain.* 1997;120:503–514.
3. Jucaite A, Fernell E, Halldin C, Forssberg H, Farde L. Reduced midbrain dopamine transporter binding in male adolescents with attention-deficit/hyperactivity disorder: association between striatal dopamine markers and motor hyperactivity. *Biol Psychiatry.* 2005;57:229–238.
4. Nakamura K, Sekine Y, Ouchi Y, et al. Brain serotonin and dopamine transporter bindings in adults with high-functioning autism. *Arch Gen Psychiatry.* 2010;67:59–68.
5. Arakawa R, Ichimiya T, Ito H, et al. Increase in thalamic binding of [^{11}C]PE2I in patients with schizophrenia: a positron emission tomography study of dopamine transporter. *J Psychiatr Res.* 2009;43:1219–1223.
6. Fowler JS, Volkow ND, Wolf AP, et al. Mapping cocaine binding sites in human and baboon brain in vivo. *Synapse.* 1989;4:371–377.
7. Wong DF, Yung B, Dannals RF, et al. In vivo imaging of baboon and human dopamine transporters by positron emission tomography using [^{11}C]WIN 35,428. *Synapse.* 1993;15:130–142.
8. Farde L, Halldin C, Muller L, Suhara T, Karlsson P, Hall H. PET study of [^{11}C] beta-CIT binding to monoamine transporters in the monkey and human brain. *Synapse.* 1994;16:93–103.
9. Ding YS, Fowler JS, Volkow ND, et al. Pharmacokinetics and in vivo specificity of [^{11}C]dl-threo-methylphenidate for the presynaptic dopaminergic neuron. *Synapse.* 1994;18:152–160.
10. Fischman AJ, Bonab AA, Babich JW, et al. [^{11}C, ^{127}I] Altropane: a highly selective ligand for PET imaging of dopamine transporter sites. *Synapse.* 2001;39:332–342.
11. Laakso A, Bergman J, Haaparanta M, Vilkman H, Solin O, Hietala J. [^{18}F]CFT ([^{18}F]WIN 35,428], a radioligand to study the dopamine transporter with PET: characterization in human subjects. *Synapse.* 1998;28:244–250.
12. Kazumata K, Dhawan V, Chaly T, et al. Dopamine transporter imaging with fluorine-18-FPCIT and PET. *J Nucl Med.* 1998;39:1521–1530.
13. Davis MR, Votaw JR, Bremner JD, et al. Initial human PET imaging studies with the dopamine transporter ligand ^{18}F-FECNT. *J Nucl Med.* 2003;44:855–861.
14. Emond P, Garreau L, Chalon S, et al. Synthesis and ligand binding of nortropane derivatives: N-substituted 2beta-carbomethoxy-3beta-(4′-iodophenyl)nortropane and N-(3-iodoprop-(2E)-enyl)-2beta-carbomethoxy-3beta-(3′,4′-disubstituted phenyl)nortropane: new high-affinity and selective compounds for the dopamine transporter. *J Med Chem.* 1997;40:1366–1372.
15. Halldin C, Erixon-Lindroth N, Pauli S, et al. [^{11}C]PE2I: a highly selective radioligand for PET examination of the dopamine transporter in monkey and human brain. *Eur J Nucl Med Mol Imaging.* 2003;30:1220–1230.
16. Jucaite A, Odano I, Olsson H, Pauli S, Halldin C, Farde L. Quantitative analyses of regional [^{11}C]PE2I binding to the dopamine transporter in the human brain: a PET study. *Eur J Nucl Med Mol Imaging.* 2006;33:657–668.
17. Hirvonen J, Johansson J, Teras M, et al. Measurement of striatal and extrastriatal dopamine transporter binding with high-resolution PET and [^{11}C]PE2I: quantitative modeling and test-retest reproducibility. *J Cereb Blood Flow Metab.* 2008;28:1059–1069.
18. Seki C, Ito H, Ichimiya T, et al. Quantitative analysis of dopamine transporters in human brain using [^{11}C]PE2I and positron emission tomography: evaluation of reference tissue models. *Ann Nucl Med.* 2010;24:249–260.
19. Shetty HU, Zoghbi SS, Liow JS, et al. Identification and regional distribution in rat brain of radiometabolites of the dopamine transporter PET radioligand [^{11}C] PE2I. *Eur J Nucl Med Mol Imaging.* 2007;34:667–678.
20. Varrone A, Steiger C, Schou M, et al. In vitro autoradiography and in vivo evaluation in cynomolgus monkey of [^{18}F]FE-PE2I, a new dopamine transporter PET radioligand. *Synapse.* 2009;63:871–880.
21. Varrone A, Toth M, Steiger C, et al. Kinetic analysis and quantification of the dopamine transporter in the nonhuman primate brain with ^{11}C-PE2I and ^{18}F-FE-PE2I. *J Nucl Med.* 2011;52:132–139.
22. Schou M, Steiger C, Varrone A, Guilloteau D, Halldin C. Synthesis, radiolabeling and preliminary in vivo evaluation of [^{18}F]FE-PE2I, a new probe for the dopamine transporter. *Bioorg Med Chem Lett.* 2009;19:4843–4845.
23. Innis RB, Cunningham VJ, Delforge J, et al. Consensus nomenclature for in vivo imaging of reversibly binding radioligands. *J Cereb Blood Flow Metab.* 2007;27: 1533–1539.
24. Leenders KL, Perani D, Lammertsma AA, et al. Cerebral blood flow, blood volume and oxygen utilization: normal values and effect of age. *Brain.* 1990; 113:27–47.
25. Hall H, Halldin C, Guilloteau D, et al. Visualization of the dopamine transporter in the human brain postmortem with the new selective ligand [^{125}I]PE2I. *Neuroimage.* 1999;9:108–116.
26. Lammertsma AA, Hume SP. Simplified reference tissue model for PET receptor studies. *Neuroimage.* 1996;4:153–158.
27. Akaike H. A new look at the statistical model identification. *IEEE Trans Automat Contr.* 1974;19:716–723.
28. Carson R. Parameters estimation in positron emission tomography. In: Phelps M, Mazziotta J, Schelbert H, eds. *Positron Emission Tomography Principle Applications for the Brain and the Heart.* New York, NY: Raven Press; 1986:347–390.
29. Seneca N, Skinbjerg M, Zoghbi SS, et al. Kinetic brain analysis and whole-body imaging in monkey of [^{11}C]MNPA: a dopamine agonist radioligand. *Synapse.* 2008;62:700–709.
30. Terry G, Liow JS, Chernet E, et al. Positron emission tomography imaging using an inverse agonist radioligand to assess cannabinoid CB1 receptors in rodents. *Neuroimage.* 2008;41:690–698.
31. Parsey RV, Slifstein M, Hwang DR, et al. Validation and reproducibility of measurement of 5-HT1A receptor parameters with [carbonyl-^{11}C]WAY-100635 in humans: comparison of arterial and reference tisssue input functions. *J Cereb Blood Flow Metab.* 2000;20:1111–1133.
32. Varrone A, Gulyas B, Takano A, Stabin MG, Jonsson C, Halldin C. Simplified quantification and whole-body distribution of [^{18}F]FE-PE2I in nonhuman primates: prediction for human studies. *Nucl Med Biol.* 2012;39:295–303.

PLOS ONE

Effects of Dopamine D_2 Receptor Partial Agonist Antipsychotic Aripiprazole on Dopamine Synthesis in Human Brain Measured by PET with L-[β-^{11}C]DOPA

Hiroshi Ito*, Harumasa Takano, Ryosuke Arakawa, Hidehiko Takahashi, Fumitoshi Kodaka, Keisuke Takahata, Tsuyoshi Nogami, Masayuki Suzuki, Tetsuya Suhara

Molecular Imaging Center, National Institute of Radiological Sciences, Chiba, Japan

Abstract

Dopamine D_2 receptor partial agonist antipsychotic drugs can modulate dopaminergic neurotransmission as functional agonists or functional antagonists. The effects of antipsychotics on presynaptic dopaminergic functions, such as dopamine synthesis capacity, might also be related to their therapeutic efficacy. Positron emission tomography (PET) was used to examine the effects of the partial agonist antipsychotic drug aripiprazole on presynaptic dopamine synthesis in relation to dopamine D_2 receptor occupancy and the resulting changes in dopamine synthesis capacity in healthy men. On separate days, PET studies with [^{11}C]raclopride and L-[β-^{11}C]DOPA were performed under resting condition and with single doses of aripiprazole given orally. Occupancy of dopamine D_2 receptors corresponded to the doses of aripiprazole, but the changes in dopamine synthesis capacity were not significant, nor was the relation between dopamine D_2 receptor occupancy and these changes. A significant negative correlation was observed between baseline dopamine synthesis capacity and changes in dopamine synthesis capacity by aripiprazole, indicating that this antipsychotic appears to stabilize dopamine synthesis capacity. The therapeutic effects of aripiprazole in schizophrenia might be related to such stabilizing effects on dopaminergic neurotransmission responsivity.

Citation: Ito H, Takano H, Arakawa R, Takahashi H, Kodaka F, et al. (2012) Effects of Dopamine D_2 Receptor Partial Agonist Antipsychotic Aripiprazole on Dopamine Synthesis in Human Brain Measured by PET with L-[β-^{11}C]DOPA. PLoS ONE 7(9): e46488. doi:10.1371/journal.pone.0046488

Editor: Kenji Hashimoto, Chiba University Center for Forensic Mental Health, Japan

Received May 31, 2012; **Accepted** September 5, 2012; **Published** September 28, 2012

Funding: This study was supported in part by a Grant-in-Aid for Molecular Imaging Program from the Ministry of Education, Culture, Sports, Science and Technology (MEXT), Japanese Government, a Grant-in-Aid for Scientific Research (C) (No. 21591587) from the Japan Society for the Promotion of Science, and a grant from the National Institute of Radiological Sciences. The funders had no role in study design, data collection and analysis, decision to publish, or preparation of the manuscript.

Competing Interests: The authors have declared that no competing interests exist.

* E-mail: hito@nirs.go.jp

Introduction

Effects of antipsychotic drugs with antagonistic property mediated by blockade of postsynaptic dopamine D_2 receptors can be evaluated by positron emission tomography (PET) studies for determining the occupancy of dopamine D_2 receptors in schizophrenia patients treated with first-generation antipsychotics, e.g., haloperidol [1,2] and second-generation antipsychotics, e.g., risperidone [3], antagonists of dopamine D_2 receptors. Recently, a new atypical antipsychotic drug acting as a partial agonist of dopamine D_2 receptors, aripiprazole, has been widely used for the treatment of schizophrenia [4]. Partial agonists of dopamine D_2 receptors can modulate the dopaminergic neurotransmission as functional agonists or functional antagonists [5].

Effects of antipsychotics on presynaptic dopaminergic functions, e.g., dopamine synthesis capacity, might also be related to their therapeutic effects. The regional activity of aromatic L-amino acid decarboxylase (AADC) in brain, indicating dopamine synthesis capacity, can be estimated using radiolabeled L-DOPA [6]. Animal studies showed significant increases and decreases in dopamine synthesis capacities by antagonists and agonists of dopamine D_2 receptors using [^{3}H]DOPA, L-[β-^{11}C]DOPA, and 6-[^{18}F]fluoro-L-DOPA, respectively [7–9]. These findings suggest that changes in presynaptic dopamine synthesis capacity might be caused by the pharmacological effects on dopaminergic autoreceptors [10]. On the other hand, an increase in dopamine synthesis capacity by administration of the partial agonist antipsychotic aripiprazole was observed in animal studies by measuring DOPA accumulation [11].

Effects of antipsychotics with antagonistic property on dopamine synthesis capacity have been studied in brains of human subjects. The acute administration of the antipsychotic drug haloperidol and the use of PET with 6-[^{18}F]fluoro-L-DOPA revealed a significant increase in dopamine synthesis capacity in healthy human subjects [12]. In contrast, in schizophrenia patients, a significant decrease in dopamine synthesis capacity after chronic administration of haloperidol was observed with PET and 6-[^{18}F]fluoro-L-DOPA [13]. Recently, we found that the antipsychotic drug risperidone could be considered to stabilize dopamine synthesis capacity in healthy human subjects, indicating that the therapeutic effects of risperidone in schizophrenia might be related to the stabilizing effects on dopaminergic neurotransmission responsivity [14]. However, the effects of the partial agonist antipsychotic aripiprazole on dopamine synthesis capacity have not yet been investigated in human subjects.

In the present study, dopamine D_2 receptor bindings and dopamine synthesis capacities at resting condition and after oral